CIVIL ENGINEERING

Lateral displacement and pile instability due to soil liquefaction using numerical model

Abdel-Salam Ahmed Mokhtar [a], **Mohamed Ahmed Abdel-Motaal** [b,*],
Mohamed Mustafa Wahidy [c]

[a] *Faculty of Engineering, Ain Shams University, Egypt*
[b] *Faculty of Engineering, Ain Shams University, Egypt*
[c] *Telecom Egypt, Cairo, Egypt*

Abstract Pile instability due to liquefaction of loose sand is considered one of the most important causes of bridge failures during earthquakes. In this study, the 3D finite element program DIANA 9.3 is implemented to study the seismic behavior of piles penetrated into liquefiable sandy soil. This model is supported by a special Line–Solid Connection element to model the interface between pile and surrounding soil.

Extensive studies were performed to investigate the effects of soil submergence, pile diameter, earthquake magnitude and duration on pile lateral deformation and developed bending moment along pile shaft. Study results show that earthquake magnitude and time duration have a particular effect on the pore water pressure generation and hence pile lateral deformation and bending moments. They also show the benefits of using relatively large piles to control the lateral displacement. Recommendations are presented for designers to perform comprehensive analysis and avoid buckling and plastic hinge failures.

© 2014 Production and hosting by Elsevier B.V. on behalf of Ain Shams University.

1. Introduction

The seismic performance of piles in liquefiable soil, their analysis and design is considered one of the most sophisticated geotechnical problems. The behavior of piles in liquefiable soil is a function of soil properties, pile properties (diameter, length and material), depth of liquefiable layer, the characteristics of applied earthquake motions, relative stiffness between piles and the surrounding soil. The dynamic design of such piles and their durability against soil liquefaction, during and after earthquakes, can be considered one of the main challenges that face structural and geotechnical engineers. Beside the excess dynamic lateral loads due to seismic excitation, excess pore

* Corresponding author. Address: Department of Structural Engineering, Faculty of Engineering, Ain Shams University, Cairo 11391, Egypt. Tel.: + 20 (2) 23054115/+ 20 (11) 25060000/+ 20 (12) 27372897; fax: + 20 (2) 23054115.
E-mail addresses: abd_mokhtar@yahoo.com (A.-S.A. Mokhtar), abdelmotal@yahoo.com (M.A. Abdel-Motaal).

Peer review under responsibility of Ain Shams University.
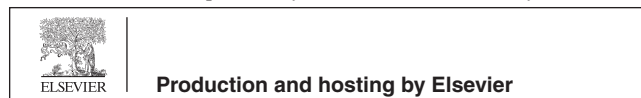
water pressures may generate and cause soil liquefaction; hence extra lateral loads are transmitted to piles. In addition to this, the pile may lose its lateral supports due to lack of soil shear strength. The conditions may become more complicated if the unsupported length of the pile is increased, which in turn can lead to the instability of the piles [1–4].

Failure of piled foundations has been observed in the majority of recent strong earthquakes. The failure of end bearing piles in liquefiable areas during earthquakes is attributed to the effects of liquefaction induced lateral spreading [1,2]. The down slope deformation of the ground surface adjacent to the pile foundation seems to support this explanation. All these theories of pile failure treat the pile as a beam element and assume that the lateral loads due to inertia and slope movement cause bending failure in the pile.

Amiri [2] presents a wide summary for historic cases of earthquakes, which induced pile damage due to lateral spreading of soil. This review presents the most famous and catastrophic pile foundation damages of bridges, where lateral movement has been observed. These lateral movements exceed 1.00 m in some cases. It includes damages during the Great Alaskan (USA, 1964), the Edgecumbe (New Zealand, 1987), the Kobe (Japan, 1995), the Luzon (Philippines, 1990) and the Niigata (Japan, 1964) earthquakes. For each earthquake, the physical nature of the event, pile foundation types, the subsurface soil condition beneath the bridge foundations and the types of the damages are discussed.

Meyersohn [1] proposed that three distinctive failure modes can be recognized in piles subjected to lateral spreads resulting from soil liquefaction. In the first one, lateral pile deflections induced by horizontal soil displacement may result in the pile reaching its bending capacity, thus developing a plastic hinge Fig. 1a. On the other hand, the lack of sufficient lateral support due to the reduced stiffness of the liquefied soil and the lateral deflection imposed on the pile may result in buckling Fig. 1b. Another type of failure is shown in Fig. 1c, where it involves excessive rigid body rotation of the pile, which is a characteristic of large diameter piles and piers. This type of response to lateral soil displacement arises primarily from a lack of sufficient restraint at the bottom of the pile, either due to an inadequate embedment length or due to low resistance of the foundation material against lateral movement. With increasing soil movement, this form of pile response may be followed by the formation of a plastic hinge at the lower interface, or by a premature collapse of the foundation due to a combination of excessive rotation and lack of lateral support.

In this study, an advanced numerical model has been used to simulate the sophisticated problem of the mutual seismic interaction between liquefiable loose sand formation and piles. The prepared numerical models are based on the finite element methodology using program DIANA 9.3 (2008). The proposed model is able to represent the soil–structure interaction system under seismic excitation and submerged conditions. Through 3D analysis, the pile is modeled as a beam element and the surrounding soil layers are modeled as solid elements. The model is supported by special 3 + 3 node Line–Solid Connection element, which is utilized to model the interface between the pile and the surrounding soil in three-dimensional configuration.

Extensive studies have been carried out to investigate the seismic interaction of the piles considering soil submergence condition, pile diameter, earthquake magnitude and duration. The characteristics of the soil dealt with are cohesionless soil having relative densities from loose to medium sand to very dense sand. Three artificial generated earthquake records have been used as the control motion at the bed-rock surface. A practical wide range of maximum base acceleration is selected ($\alpha = 0.05$–0.20 g), considering earthquake durations of 10, 20 and 40 s. Both pile lateral deformation and the developed bending moment along pile shaft are studied. Recommendations and conclusions are presented for the designer to avoid both buckling and plastic hinge failures.

2. Previous studies

Most previous studies performed and examined centrifuge tests as an experimental modeling technique. On the other hand, a few number of researches deal with the numerical solution approach to investigate the pile response and behavior in such conditions.

Meyersohn [1] conducted an analytical study of pile foundation response to lateral spreads using computer code B-STRUCT. The analysis results have been compared with field observations of pile deformations underground failure conditions. The results of the study have been used to develop dimensionless charts. These charts allow the determination of the failure mechanisms of piles with respect to the relative stiffness and pile axial load. Another set of charts have been developed to determine surface soil displacements related to excessive bending conditions and plastic hinge formation.

Popescu and Prevost [3] showed that the VELACS project offers a good opportunity to verify and validate various
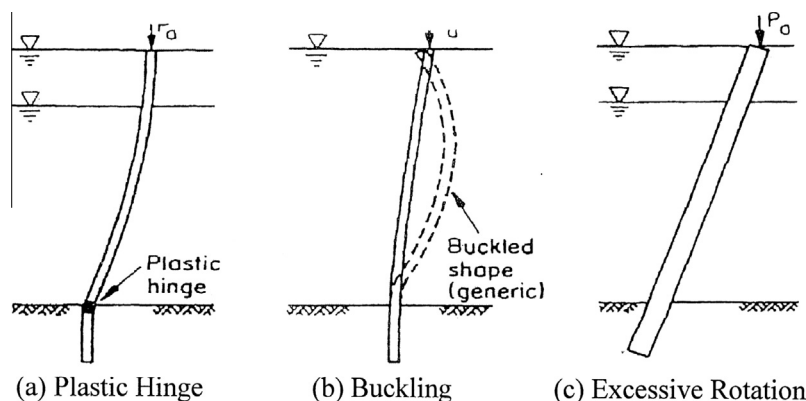

(a) Plastic Hinge   (b) Buckling   (c) Excessive Rotation

Figure 1 Pile failure mechanisms (after Meyersohn, 1994 [1]).

analytical procedures for numerical simulation of soil liquefaction, by comparing the "class A" predictions with the centrifuge experimental results. The comparison is made in terms of: (1) the root mean square error of the predictions with respect to the mean of the experimental results and (2) the size of a confidence interval centered at the predicted value which contains the estimated true value of the experimental results with 75% probability.

Wilson et al. [4] carried out centrifuge tests on single pile and pile group supported structure in liquefied sand. Their works confirmed that the lateral p–y resistance of liquefied soil is a complex phenomenon and is significantly affected by relative density, cyclic degradation, excess pore pressures, phase transformation behavior, prior displacement history and loading rate. They reported that there is a considerable uncertainty in any simplified representation of p–y characteristics of liquefied soil and this uncertainty must be considered in design.

Bhattacharya [5] reviewed the current design methods and the underlying mechanism (bending) behind the design methods. Critical remarks are made on the understanding of pile failure citing the example of the well-known failure of Showa Bridge. An alternative mechanism of pile failure was proposed. This mechanism, based on pile buckling, was verified using dynamic centrifuge tests.

Ashour and Norris [6] proposed a new analysis procedure for assessing the lateral response of a pile in liquefiable sand under dynamic loading conditions. Their procedure is able to predict the degradation in pile response and soil resistance due to free field excess pore water pressure generated by earthquake shaking. It is able to account for the near field excess pore water pressure generated by lateral loading transmitted from the superstructure. It is also capable of predicting the response of laterally loaded single pile and the associated modulus of subgrade reaction.

Abdoun et al. [7] performed eight centrifuge experiments on models of vertical single piles and pile groups subjected to earthquake-induced liquefaction and lateral spreading. The piles were penetrated into loose liquefiable Nevada sand with 40% relative density. The centrifuge results were used to calibrate two limit equilibrium methods for engineering evaluation of bending moments acting on pile in the field.

Ilyas et al. [8] conducted a series of centrifuge model tests to examine the behavior of laterally loaded pile groups in normally consolidated and over-consolidated clay. The test results established that the pile group efficiency reduces significantly with increasing number of piles in a group. It is found that the outer piles in the row carry significantly more load and higher bending moment than those of the inner piles.

Rollins et al. [9] have performed lateral load test on a full scale single pile and pile group following blast-induced liquefaction to evaluate pile–soil–pile interaction effects. The test results showed that after liquefaction the behavior of pile group is almost the same as that for single pile. The p–y curves stiffened with depth as the excess pore pressure ratio decreased. Their work yielded equations for p–y curves in liquefied sand that was able to account for the effect of variations in pile diameter.

Weaver et al. [10] conducted a full scale lateral load test on a 0.60 m cast in steel shell pile in sand liquefied and controlled blasting. The dynamic p–y curves were compared with the static p–y curves. The study showed that the shape of p–y curves for liquefied sand is significantly different from standard p–y curves. As a result, the modified standard p–y curves do not adequately model the liquefied soil response.

Wahidy [11] studied the stability of piles penetrated into liquefiable soil using numerical finite elements model. The numerical models were prepared by the finite element program DIANA 9.3 [12]. Study results showed that earthquake duration, pile diameter, pile length and submergence condition have major effects on the maximum absolute bending moments along pile shaft. Study established that for ratios between pile length and its diameter ($L/D < 30$), the stress acting on pile is less than the Euler's stresses, so buckling failure will not take place. At this situation, the expected failure mechanisms are plastic hinge formation or excessive rotation. Although this study established the condition of buckling failure, it does not deeply study plastic hinge and excessive rotation failure mechanism.

Madabhushi et al. [13] provided a logical framework for understanding the basics of single pile and pile group design, liquefaction and the effect of earthquake loading and liquefaction on the axial and lateral loads transmitted to piles foundations. This textbook also provides a framework for understanding the effects that loss of bearing and lateral restraint in saturated sandy soils subject to cyclic loading have on the capacity of pile foundations. By combining earthquake loading in liquefiable soils with mechanisms that reduce pile capacity, rational process is developed for quantifying loads and capacity reduction into a design process.

Li et al. [14] carried out numerical simulation of pile–soil interaction considering saturated sand liquefaction under earthquake using OpenSees program. In this model, the soil was divided into soft clay soil and saturated sand, where the single pile was installed into the soil. The results showed that the pore water pressure rises and the soil liquefies as vibration time increases. With the nonlinear characteristics of the soil, the stiffness, bearing capacity and the acceleration response of the soil and the pile decreased, while the displacement response of the soil increased.

3. Numerical modeling

In the absence of centrifuge tests or full scale tests, it is very useful to use the numerical solution approach to model such sophisticated geotechnical problems. The problem of soil liquefaction could be treated using finite element approach. Single pile, piles group, pile caps and superstructure can be modeled and analyzed in many soil conditions under seismic load. In the current study, the integral finite element program DIANA 9.3 (2008) has been implemented to study the seismic behavior of single pile penetrated into liquefiable soil. The pile is modeled as beam element and the surrounding soil layers are modeled as solid elements, in 3D modeling configuration. Plane interface elements are used to model the relationship between pile shaft surface and soil.

Mutual cooperation between the research team and TNO – DIANA members was done to enhance the model. In the initial stages of the study, the results were not accurate and not compatible with previous published results obtained using centrifuge tests. Accordingly, TNO – DIANA crew developed special 3 + 3 nodes, Line–Solid Connection element, which utilized to model the interface between the pile and the surrounding soil in three-dimensional configuration.

This special element is available in the newer release DIANA 9.3 [12]. The new element facilitates the problem modeling and the results become more accurate, reliable and compatible with centrifuge tests results. In the following sections the model details will be presented.

3.1. Good analysis requirements

Currently, analysis including the effects of ground motions variation with depth has been developed using the finite element method [15–19]. Not all finite element analysis of soil structure interaction provides adequate evaluations of seismic response, as they could be performed with different degrees of approximation or sophistication. The basic requirements for a good analytical procedure could be summarized as follows:

1. The model should be represented in 3-D configuration.
2. The analysis should be performed under transient dynamic conditions.
3. The analysis should consider the non-linear behavior of soil and its viscous damping characteristics.
4. Variation in soil characteristics with depth should be considered.
5. For piles, the analysis should consider the variation in ground motion with depth.
6. The analysis should be capable of considering the pore water pressure generation in the saturated soil under restrained pore water conditions and soil liquefaction.
7. The analysis should consider the interface between the pile and the surrounding soil.
8. Finally, the solution aims to predict the displacement and the moment on the pile cross-section concerning the liquefaction of soil layers.

4. Methodology algorithm

The system of governing equations for a transient dynamic problem at time t is generally written as:

$$M\ddot{U} + C\dot{U} + f_{in}(u, \dot{u}, \varepsilon, \dot{\sigma}, t, \ldots) = f_{ex}(t) \qquad (1)$$

where M is the mass matrix, C the damping matrix and f_{ex} is the external force vector or right-hand side vector of forcing functions. Furthermore, $\ddot{U}$ and $\dot{U}$ are the resulting acceleration and velocity vectors, respectively. Vector f_{in} is the internal set of forces opposing the displacements, and ε and σ are the strain and stress fields, respectively.

For geometrical or physical nonlinear analysis or both, f_{in} must be calculated for the actual stress distribution satisfying all nonlinear conditions.

$$f_{in} = \int B^T \sigma \qquad (2)$$

For the transient response of a nonlinear analysis, the solution of the second order differential equation, Eq. (1) is obtained by direct time integration techniques. The solution for the dynamics problem will be determined at a number of discrete time points: $t_0, t_1, t_2,..., t - \Delta t, t, t + \Delta t,..., T$.

4.1. Integration scheme

There are various types of integration schemes, which are available for transient dynamic analysis. Newmark method, Euler Backward method, Hilber-Hughes-Taylor method, Runge-Kutta methods and the Wilson – θ method are available integration schemes in DIANA 9.3 [12]. All of these methods have been tested and was established that the most stable and suitable one for liquefaction analysis is the Wilson – θ method. This method conducts good results without ill-conditions or sudden stopping for the analysis process. The Wilson - θ method is basically an extension of the Newmark scheme with $\gamma = 1/2$ and $\beta = 1/6$ (for which the Newmark method is conditionally stable). In the Wilson – θ method, the acceleration is assumed to vary linearly in time from t' to $t' + \theta \Delta t'$ with $\theta \geqslant 1$. Considering this assumption, the following equations could be driven for [$t' + \theta \Delta t'\ \dot{U}$ and $t' + \theta \Delta t'\ \ddot{U}$]:

$$t' + \theta\Delta t'\ddot{U} = \frac{6}{\theta^2\,\Delta t'^2}\left(t' + \theta\Delta t'_u - t'_u\right) - \frac{6}{\theta\Delta t'}t'\dot{u} - 2t'\ddot{u} \qquad (3)$$

$$t' + \theta\Delta t'\dot{U} = \frac{3}{\theta\Delta t'}\left(t' + \theta\Delta t'_u - t'_u\right) - 2t'\dot{u} - \frac{\theta\Delta t'}{2}t'\ddot{u} \qquad (4)$$

The dynamic equilibrium equation is considered at $t' + \theta\Delta t'$.

$$^{t'+\theta\Delta t'}M\,^{t'+\theta\Delta t'}\ddot{U} + {}^{t'+\theta\Delta t'}C\,^{t'+\theta\Delta t'}\dot{U} + {}^{t'+\theta\Delta t'}f_{in} = {}^{t'+\theta\Delta t'}f_{ex} \qquad (5)$$

In this equation the external load vector on the right-hand side is just like the acceleration assumed to vary linearly in the time interval $t' \rightarrow t' + \theta\Delta t'$.

$$^{t'+\theta\Delta t'}f_{ext} = {}^{t}f_{ex} + \theta({}^{t'+\Delta t'}f_{ex} - {}^{t}f_{ex}) \qquad (6)$$

4.2. Base excitation

The dynamic response such as displacements, stresses of a finite element system may not only be induced by prescribed loadings, but also by motions of its supported points. A base excitation is applied at model base (bed-rock surface). By expressing the response relative to a fixed ground point, the equation of motion, Eq. (1) may be written in the form:

$$M\ddot{U} + C\dot{U} + f_{in}(u, \dot{u}, \varepsilon, \sigma, t, \ldots) = -M\ddot{U}_b(t) \qquad (7)$$

where u is now the relative response and the external loading f_{ex} has been replaced by an effective loading due to the base excitation, in which $\ddot{U}_b$ represents the applied base acceleration vector.

4.3. Model elements

4.3.1. Soil element

Eight-node isoparametric 3D solid brick element is used to model the soil strata. The basic variables in the nodes of solid elements are the translations u_x, u_y and u_z in the local element directions. The Bowl liquefaction constitutive model [11,12,20] was developed on behalf of the Japanese Liquefaction User Group in 1998. This fully coupled model is implemented in the analysis to model the soil strata. Some basic assumptions of the model are considered as follows:

1. The model is not frame invariant. It assumes predominant horizontal shearing, working in local x direction for two-dimensional analysis and in local x or y direction for three-dimensional analysis. Furthermore, it assumes that dilatancy will only cause normal plastic strain in the vertical direction of gravity, where that direction is assumed to be the local y axis in two-dimensional analysis and the local z-axis in three-dimensional analysis. The deviatoric behavior of the Bowl model is modeled with a modified Ramberg–Osgood model:

$$\gamma_{xy} = \frac{\sigma_{xy}}{G}(1 + \alpha|\sigma_{xy}|^{\beta}) \qquad (8)$$

where the shear strain in the xy-direction is determined by the linear shear strain $\frac{\sigma_{xy}}{G}$ and the actual shear stress level through the factor $(1 + \alpha|\sigma_{xy}|^{\beta})$. The actual shear modulus "G" is given by:

$$G = G_{ref}\left(\frac{\sigma'_m}{\sigma'_{m.ref}}\right)^{1/2} \qquad (9)$$

where σ'_m is the mean effective pressure and G_{ref} is the reference shear modulus at the reference mean effective pressure $\sigma'_{m.ref}$. The coefficients α and β are given by:

$$\alpha = \left(\frac{2}{\gamma_{0.50}G}\right)^{\beta} \quad \text{and} \quad \beta = \frac{2\pi h_{max}}{2 - \pi h_{max}} \qquad (10)$$

where h_{max} is the maximum damping ratio of the soil, and $\gamma_{0.50}$ is the reference shear strain at the value $[G/G_{ref} = 0.5]$.

2. To simulate the non-linear behavior of soil, unloading and reloading is described by Masing's rule, which states that the unloading and reloading curves are given by:

$$\frac{\gamma_{xy} + \gamma_{rev}}{2} = \frac{\sigma_{xy} + \tau_{rev}}{2G}\left(1 + \alpha\left|\frac{\sigma_{xy} + \tau_{rev}}{2}\right|^{\beta}\right) \qquad (11)$$

In which $(\gamma_{rev}, \tau_{rev})$ are the coordinates of the current reversal point in the stress–strain curve, Fig. 2.

3. In the Bowl model, the total volumetric strain ε_{vol} is decomposed into a dilatancy component ε^s_{vol} due to cyclic shear loading and an elastic component ε^c_{vol} due to changes in the effective mean stress:
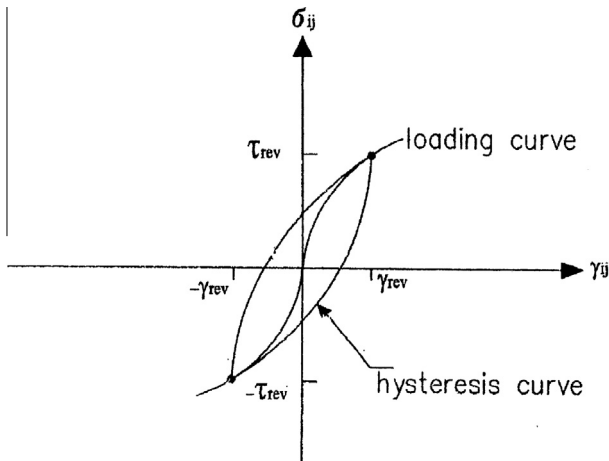

Figure 2 Ramberg–Osgood model with Masing's rule [12].

$$\varepsilon_{vol} = \varepsilon^s_{vol} + \varepsilon^c_{vol} \qquad (12)$$

The dilatancy component ε^s_{vol} comprises two components:

$$\varepsilon^s_{vol} = \varepsilon^{\Gamma}_{vol} + \varepsilon^{G^*}_{vol} \qquad (13)$$

where the dilatancy component $\varepsilon^{\Gamma}_{vol}$ models the increasing volume due to shearing loading as a function of the equivalent shear strain Γ as follow:

$$\varepsilon^{\Gamma}_{vol} = -A\Gamma^B \qquad (14)$$

where A and B are soil parameters.

The dilatancy component $\varepsilon^{G^*}_{vol}$ describes the compaction of the material due to shear loading as a function of the cumulative shear strain G^* as follow:

$$\varepsilon^{G^*}_{vol} = -\frac{G^*}{C + DG^*} \qquad (15)$$

where C, D are soil parameters and

$$G^*(t) = \int_0^t G^* \cdot dt \qquad (16)$$

The elasticity component ε^c_{vol} is given by the compression relationship

$$\varepsilon^c_{vol} = -\frac{C_s}{1 + e_o} \cdot \log\frac{\sigma'_m}{\sigma'_{mo}} \qquad (17)$$

In which e_o is the initial void ratio and C_s is the swelling index. The initial effective mean stress is denoted σ'_{mo} and the effective mean stress at any time t is σ'_m.

The excess pore water pressure $\Delta\mu$ is obtained from the condition of no volumetric strain increment under the undrained condition [21]. Accordingly, $\Delta\mu$ and the pore water pressure ratio r_u could be estimated as follow:

$$\Delta\mu = \sigma'_{mo} - \sigma'_m \qquad (18)$$

$$r_u = \frac{\Delta\mu}{\sigma'_{mo}} \qquad (19)$$

4.3.2. Pile elements

Two-node three-dimensional beam elements are used to model the single pile. The basic variables are the translations u_x, u_y and u_z and the rotations φ_x, φ_y and φ_z at the nodes.

4.3.3. Interface elements

Fig. 3 shows special 3 + 3 nodes, Line–Solid Connection element, which was utilized to model the interface between the pile and the surrounding soil in three-dimensional configuration. This element is only applicable in models for three-dimensional bond–slip analysis. It represents the bond area between the pile and its surrounding soil. The local xyz axes for the displacements are evaluated in each node with x in the tangential direction and z in the normal direction. The interface shear stiffness value, D_{tt} can be defined according to the following equation:

$$D_{tt} = (A_r^2/t_d)(E_{soil}/(2(1 + v_{soil}))) \qquad (20)$$

The interface normal stiffness value D_{nn} can be defined according to the following equation:
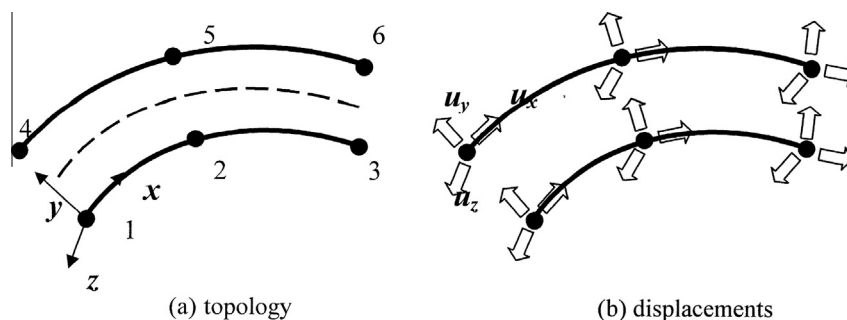
$$D_{nn} = fD_{tt} \qquad (21)$$

Figure 3   Special 3 + 3 nodes, Line–Solid Connection element [12].

where E_{soil} is the soil modulus of elasticity and v_{soil} is the soil Poisson's ratio. Factor A_r is a reduction factor to render the soil–structure interface, which is weaker and more flexible than the surrounding soil formation (A_r may range from 0.5 to 1.0). Factor t_d is a small distance representing the virtual thickness of the interfaces and f is a multiplication factor that could vary from 10 to 100.

4.4. Model verification and validation

Uzuoka et al. [22] presented a comparison between shake table test and numerical analysis using DIANA program. The key objective was to assess the accuracy of the 3-D effective stress analysis in predicting liquefaction-induced ground flow and the behavior of piles in liquefying soils. Results indicated that the constitutive model provides reasonably good accuracy in predicting the excess pore pressures and ground deformation, thus allowing proper evaluation of the soil–pile interaction effects. In general, the computed ground response was found to be in good agreement with that observed in the experiments including the deformation pattern, development of excess pore pressures. The computed response of the foundation piles including both lateral displacements and bending moments was in very good agreement with the response measured in the experiment.

Through a comprehensive study by Wahidy [11] and Mokhtar et al. [20], the model has been verified and checked by comparing analytical results on pile foundation with laboratory centrifuge test results done by Abdun et al. [7]. Considering the maximum developed bending moment time history along pile shaft, analysis results showed a very good agreement between analytical model and centrifuge test results.

Tolon [23] carried out a comparative study on computer aided liquefaction analysis. This study included 23 finite element and finite difference programs. According to study results, DIANA program was classified as one of the best three programs capable of solving 3D liquefaction potential in detailed models.

5. Lateral movement and pile instability study

Based on the above mentioned numerical model, about two hundred finite element models have been prepared to investigate the seismic behavior of axially loaded single concrete piles installed into liquefiable sand soil. Fig. 4 shows the soil stratification and the numerical model for such case study. Both lateral movements of a pile and its stability are the study concern. The pile is assumed carrying a concentrated mass applied on its top end. This concentrated mass is assumed to be as a simple simulation of pile load share from the superstructure weight (exerting 4.0 N/mm^2 static normal stress along pile shaft). Extensive studies have been carried out to investigate the effect of many parameters such as: maximum base acceleration ($\alpha = 0.05$, 0.10, 0.15 and 0.20 g), earthquake duration (10, 20 and 40 s), pile diameter ($D = 0.4$, 0.6, 1.0 and 1.5 m), pile length ($L = 10.0$, 12.0, 14.0 and 16.0 m), submergence condition (fully dry and fully submerged) and thickness of liquefiable layers (6.5 m or 12.0 m). The effect of each parameter on the stability of piles has been also investigated. Recommendations and conclusions are presented to the designer to avoid both buckling and plastic hinge failures. In the following sections, the model applications and results are presented:
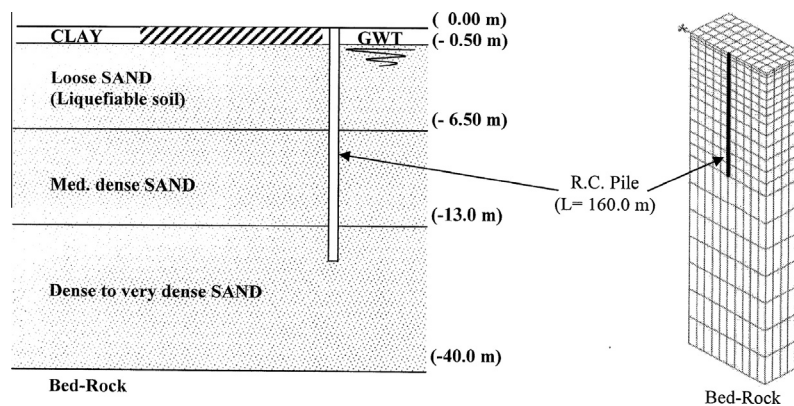

Figure 4   The proposed soil stratification and half-sectional elevation numerical Model.

Table 1 Physical and mechanical soil properties.

Soil type	Identification	SPT-N value	γ_b^* (kN/m³)	γ_{sub}^* (kN/m³)	E^* (kN/m²)	Dr^* (%)	φ^a (°)
1	Loose sand (dry)	8–13	17		3.0E4	35	32
2	Loose sand (saturated)	8–13	18	8	2.5E4	35	32
3	Medium dense sand	23–30	19	9	1.0E5	60	35
4	Dense sand	45 and more	20	10	2.0E5	85	40

ᵃ Values are estimated according to the Egyptian code of soil mechanics and foundations (202/2001) [24].

5.1. Soil formations and their mechanical properties

The top soil formation consists of impervious clay layer (0.50 m thickness), followed by a liquefiable loose sand formation (6.5 m or 12.0 m). The third layer is a medium dense sand layer (6.0 m thickness) rested on a deep layer of dense to very dense sand. The soil stratification is shown in Fig. 4. Physical and mechanical soil properties are shown in Table 1, where these values are estimated according to the Egyptian Code of Soil Mechanics and Foundation (202/2001) [24]. It is very important to mention that the adopted soil stratification is similar to the prevailing soil condition at some areas at the south west of Cairo. These areas suffered from liquefaction after Dahshour Earthquake 1992, Cairo, Egypt.

5.2. Ground motion (base excitation)

Based on previous numerical studies by Abdel-Motaal [18], three artificial generated earthquake records (10, 20 and 40 seconds) have been used as a control motion at the base of the dense sand formation (bed-rock surface). These records are based on the standard response spectrum, Uniform Building Code (1994), where Fig. 5 shows the response spectrum for the used records in comparison with standard response spectrum of rock. For analysis purposes, the records were scaled to apply maximum base acceleration (α = 0.05, 0.10, 0.15 and 0.20 g).

6. Result analyses

6.1. Lateral displacement of piles

6.1.1. Effect of pile diameter (flexural rigidity)

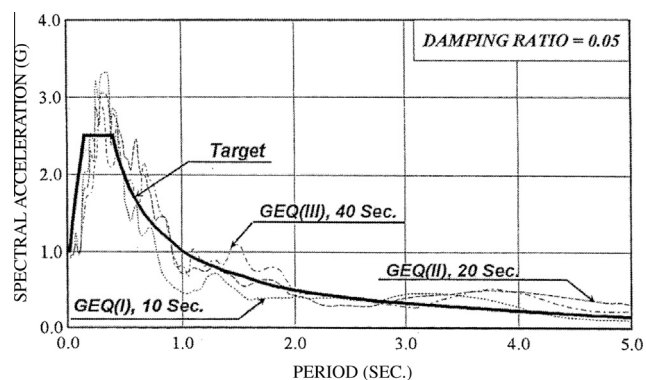Figs. 6 and 7 show the pile lateral displacements profile considering two extreme cases of pile diameters (D = 0.4 and
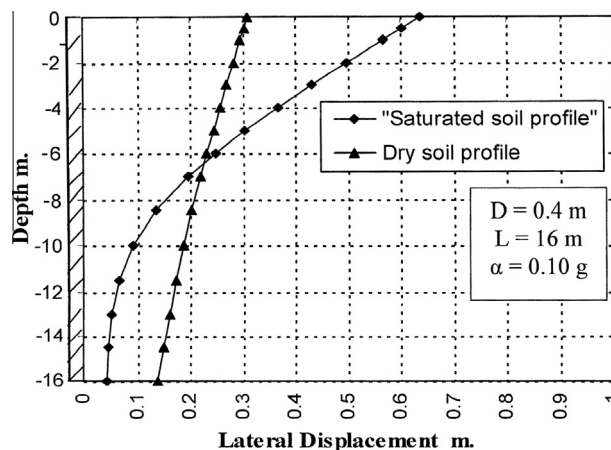
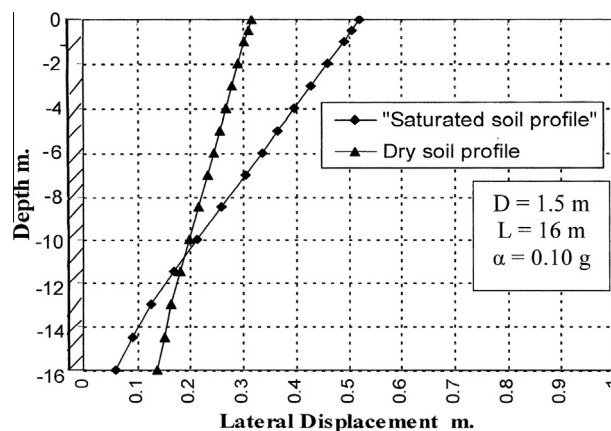**Figure 6** Profiles of lateral displacement (L = 16 m, D = 0.4 m, α = 0.10 g).

Figure 7 Profiles of lateral displacement (L = 16 m, D = 1.5 m, α = 0.10 g).

1.50 m). The profiles are plotted considering (1) dry situation and (2) fully submerged (i.e., Ground Water Table, GWT on the top of loose sand formation). Examining these figures, the following results could be established:

1. In general, the lateral displacement of a pile due to seismic excitation is relatively high due to the low lateral resistance of the upper loose sand formation. This note is mentioned in all case studies for both dry and fully saturated soil.
2. Figs. 6 and 7 show a comparison between the lateral displacement of a pile in both dry and fully submerged conditions. The two figures show the results of the smallest and largest studied pile diameter sizes

Figure 5 Acceleration response spectrum of the used generated earthquakes compared with the UBC, 1994 (after Abdel-Motaal, 1999) [18].

(*D* = 0.40 and 1.50 m), where it is found that the maximum lateral displacement of a pile's top end of a totally submerged case is usually greater than that of a full dry case. This note could be clarified as the liquefaction of loose sand causes a reduction in its shear resistance and consequently its lateral resistance (earth support).

3. Considering the deformation shape (lateral displacement) of the piles, it is clear that the deformation of the small diameter piles (Fig. 6) is highly affected by the developed flexural moment at the pile sections (behavior of horizontally loaded cantilever flexible pile). On the other hand, Fig. 7 shows the rigid body rotation pattern for a relatively large rigid pile (refer to failure mechanism, Fig. 1).

4. In general, the lateral deformation of small diameter piles is greater than that of large diameter piles. This result reflects the benefits of using large diameter piles to efficiently reduce the lateral movement of the foundation and hence the superstructure.

6.1.2. Effect of base acceleration

Extensive studies have been carried out to investigate the effect of the maximum base acceleration (α = 0.05, 0.1, 0.15 and 0.20 g). Study results are plotted in Figs. 8 and 9, considering the two extreme values of piles diameters (*D* = 0.4 and 1.5 m, respectively). Study results show that:

1. Base acceleration is associated with the increase in the estimated lateral displacement, in a nonlinear behavior. The above-mentioned standard patterns of lateral deformation for both flexible pile (*D* = 0.4 m) and rigid pile (*D* = 1.5 m) can be mentioned.

2. Figs. 10 and 11 show lateral displacement profiles, considering a wide range of pile diameters under the effect of base excitation (α = 0.1 and 0.20 g), respectively. In general, study results show that the lateral displacement of the pile top end for rigid piles is less than that for flexible piles, especially in case of high base excitation. This result reflects the benefits and importance of using large diameter rigid piles to control the lateral movements of the pile's top end.
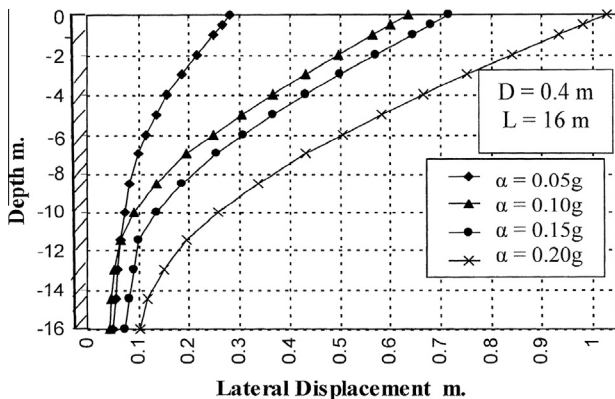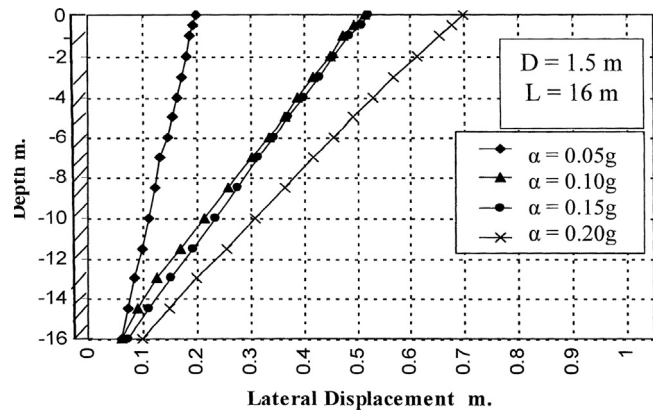

Figure 9 Profiles of lateral displacement, considering different base excitation values (Case of fully saturated soil, *L* = 16 m and *D* = 1.50 m).

3. Fig. 12 is plotted to show a combination between the effect of pile diameter and the maximum applied base acceleration on the maximum lateral displacement of the pile. Upon examining this figure, the following can be established:

    (i) The lateral displacement is highly affected by the maximum base acceleration (i.e., the earthquake associated energy).

    (ii) Pile diameter has a significant effect on reducing the lateral displacement, especially for relatively small and medium size pile diameters (up to 1.0 m diameter). For pile diameters greater than 1.0 m, the effect of pile diameter is so limited. Accordingly, 1.0 m pile diameter may be considered as optimal and economical size for such case study.

6.1.3. Effect of earthquake time duration

As mentioned before, studies have been carried out considering three artificial generated earthquake records, GEQ (I, II and III). The above mentioned results were obtained considering the base excitation of the generated Earthquake GEQ (II), where the time period is 20 seconds. Extensive studies have
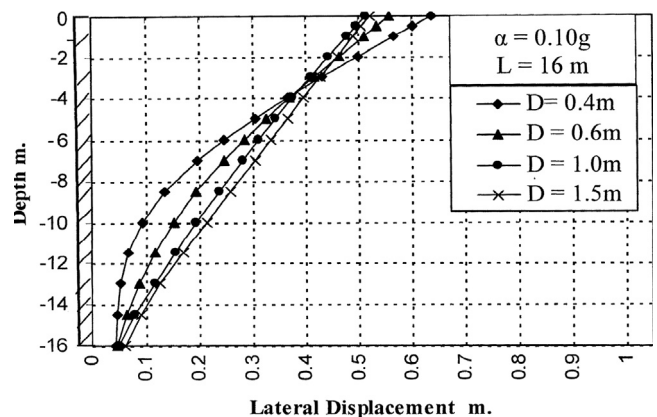

Figure 8 Profiles of lateral displacement, considering different base excitation values (Case of fully saturated soil, *L* = 16 m and *D* = 0.40 m).
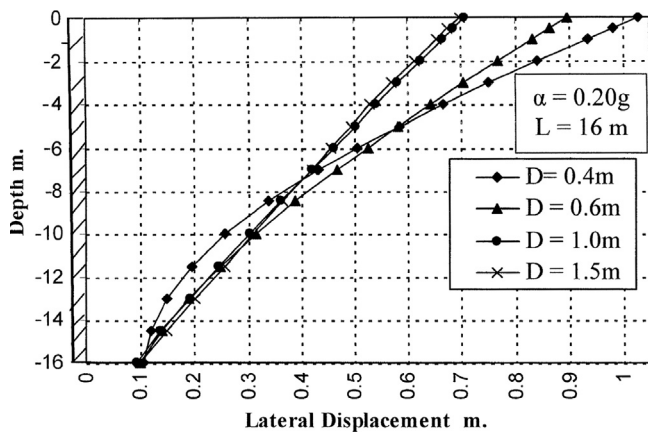

Figure 10 Profiles of lateral displacement, considering different pile diameters (*L* = 16 m and α = 0.10 g).

Figure 11 Profiles of lateral displacement considering different pile diameters ($L = 16$ m and $\alpha = 0.20$ g).
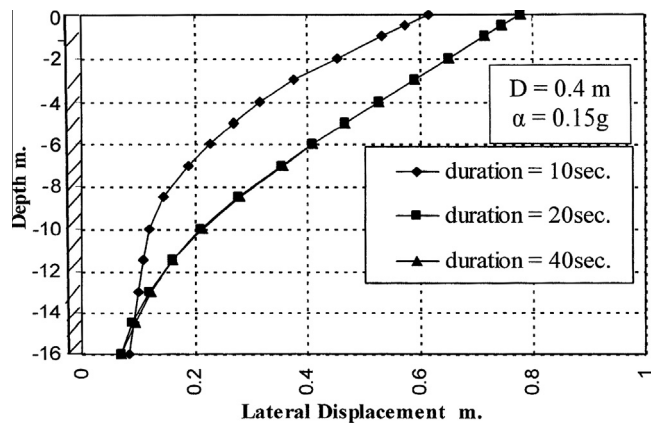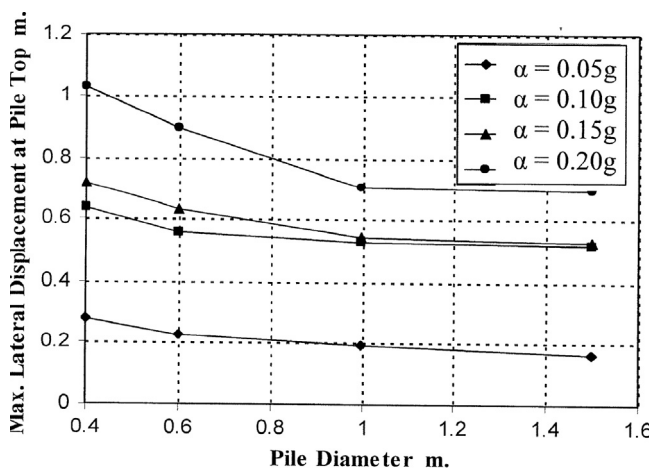

Figure 12 Relation between Max. lateral displacement and pile diameters, under the effect of different base excitation ($L = 16$ m).

Figure 13 Profiles of lateral displacement considering different earthquake durations ($L = 16$ m and $D = 0.40$ m).
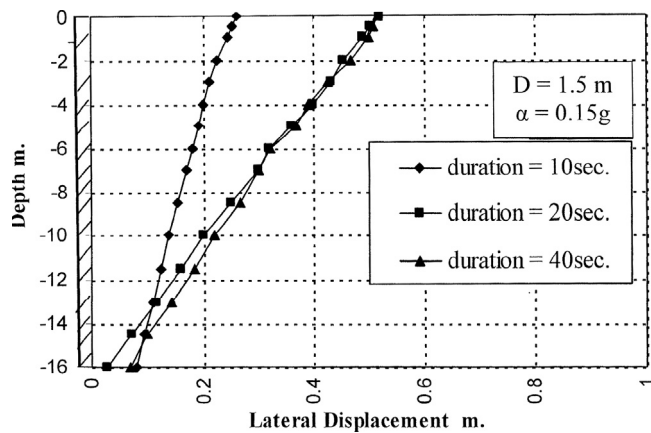

Figure 14 Profiles of lateral displacement considering different earthquake durations ($L = 16$ m and $D = 1.50$ m).

been carried out considering both GEQ (I) and GEQ (III) where the time periods are 10 and 40 s, respectively. The following can be established:

1. Figs. 13 and 14 show the lateral displacement profiles considering pile diameters ($D = 0.4$ and 1.5 m), under the effect of the three base excitation records. In general, it was mentioned that there is a considerable difference between the results of using the short time period, GEQ (I) and the other relatively long time period records, GEQ (II and III).

2. To investigate and clarify the effect of the earthquake duration, another group of curves, Figs. 15 and 16, are plotted to show the relation between the pore water pressure ratio r_u and time, where r_u is defined numerically as the ratio between the excess water pressure due to dynamic excitation and the effective normal stress at the studied level. It means that if ($r_u = 1.0$), full liquefaction will take place. On the other hand, values of ($r_u < 1.0$) indicates the condition of partial liquefaction (partial loss of shear strength). Fig. 15 shows the results and behavior of the upper loose sand formation (at mid point through layer height) considering base

excitation ($\alpha = 0.05$, 0.10, 0.15 and 0.20 g). Similarly, Fig. 16 shows the pore water pressure time history at point located 2.0 m below the surface of the medium dense sand layer. Study results show that:

(i) Ten (10) seconds time period may not be sufficient to reach the peak values of the pore water pressure ratio, especially in case of low base excitation ($\alpha = 0.05$ g). Accordingly, the generated dynamic water pressure was not sufficient to fully liquefy the loose sand layer and hence the soil does not completely lose its shear strength. As a result, the lateral displacement for such case of short time duration recorded relatively low values of lateral deformations.

(ii) Considering the loose sand formation, it is clear that the dynamic energy of high base acceleration ($\alpha = 0.20$ g) could rapidly develop the dynamic water pressure and reach the full liquefaction situation after nearly 3 seconds. On the other hand, low base excitation could reach the same situation after relatively longer time (about 13 s).

(iii) Fig. 16 shows the results of the medium sand formation located between levels (-6.50 and -13.00 m). Study results show that the peak values of water pressure ratios could be developed after relatively long time
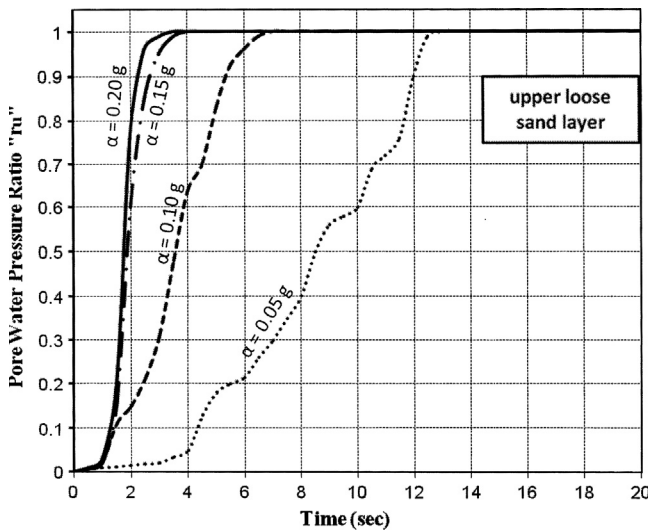
Figure 15 Relation between time and pore water pressure ratio r_u at mid point of the upper loose sand layer.
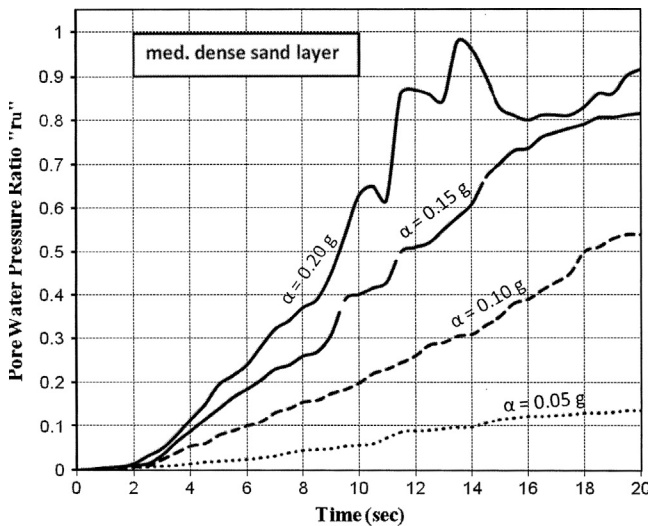

Figure 16 Relation between time and pore water pressure ratio r_u at point located 2.0 m below the surface of the medium dense sand layer.

periods (14–20 s). In general, the condition of full lique-faction is not observed when the values of ($r_u < 1.0$). Moreover, the maximum recorded values of r_u are directly proportional to the maximum base excitation (i.e., the earthquake associated energy).

(iv) In general, results indicate that energy associated with 20 s duration time is sufficient to reach the peak values of the pore water pressure ratio. Accordingly, there is no difference between results using both 20 and 40 s time period.

6.2. Soil deformation around the pile

Fig. 17 shows the soil deformations around the pile (at the level of pile top end), considering ($D = 1.5$ m and $\alpha = 0.10$ g). Upon examining this figure, the following can be established:

1. There is a good compatibility between pile deformation and the adjacent soil. This note confirms that the model works well and truly captures the 3D effects during liquefaction.
2. Pile existence has a considerable effect on reducing the lateral deformation of the adjacent soil in comparison with the far soil elements (about% reduction).

6.3. Developed bending moments along pile shaft

Extensive studies have been carried out to estimate the exerted bending moment along pile shaft, considering a wide range of variables. Figs. 18 and 19 show the bending moment profile along pile shaft (16.0 m length), under dynamic excitation of GEQ (II). The effect of the wide range of the maximum base acceleration is examined. The results of the two extreme conditions of the maximum base acceleration ($\alpha = 0.05$ and 0.20 g) are plotted in Figs. 18 and 19, respectively. Study results show that:

1. In general, the pattern of the exerted bending moment is similar to bending moment diagram of cantilever wall. Its maximum value is located within the depth of the medium sand layer, where the soil passive resistance could be generated.
2. The exerted bending moment is highly related and directly proportional with pile diameter. This observation could be clarified as increasing pile diameter has a double effect on the exerted bending moments. The first one concerns pile flexural rigidity and hence its capability to resist lateral deformation of the liquefied upper loose sand formation. The second factor is related to the increase of the contact area between pile and soil, leading to increase the total mutual soil passive resistance, along with pile fixation length (at deep soil layers).
3. Fig. 20 shows the effect of the earthquake magnitude (maximum base acceleration) on the maximum developed bending moments. It is clear that the maximum base acceleration has a considerable effect at zone of relatively low base accelerations (up to $\alpha = 0.10$ g). As mentioned before, these relatively low base accelerations have not sufficient dynamic energy to exert full liquefaction ($r_u < 1.0$). For higher values ($\alpha > 0.10$ g), full liquefaction ($r_u = 1.0$) could take place and hence no lateral resistance from the upper liquefied loose sand layer. At this condition, the effect of increasing the earthquake magnitude is limited, especially for large piles.

6.4. Expected failure mechanism

The maximum absolute developed bending moment along with pile shaft and its diameter are plotted in Fig. 21, considering the two extreme maximum base accelerations ($\alpha = 0.05$ and 0.20 g). Another group of curves are shown on the same figure. These curves represent the pile section flexural moment capacity (allowable bending moment, according to the working stress design method). Three curves are plotted considering practical range of reinforcement ratio ($As/Ac = 1.0\%$, 1.5% and 2.0%), where As is the total area of steel reinforcement bars and Ac is the cross-sectional area of the concrete pile. From a design point of view, the intersection between the
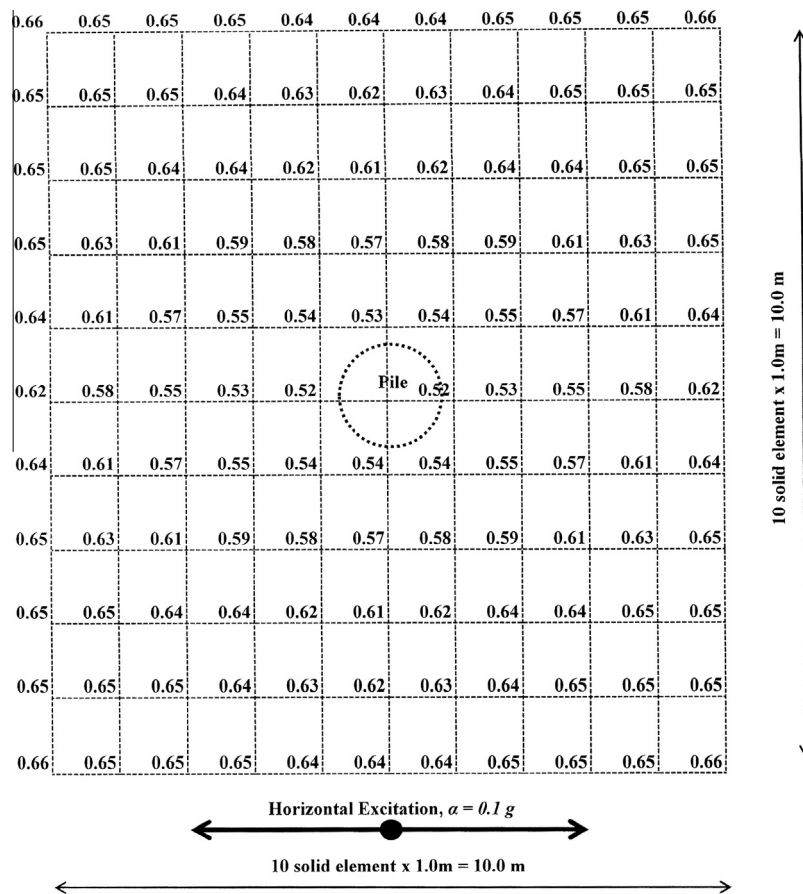
Figure 17 Plan showing soil deformations around the pile (at level of pile's top end), considering ($D = 1.5$ m and $\alpha = 0.10$ g).
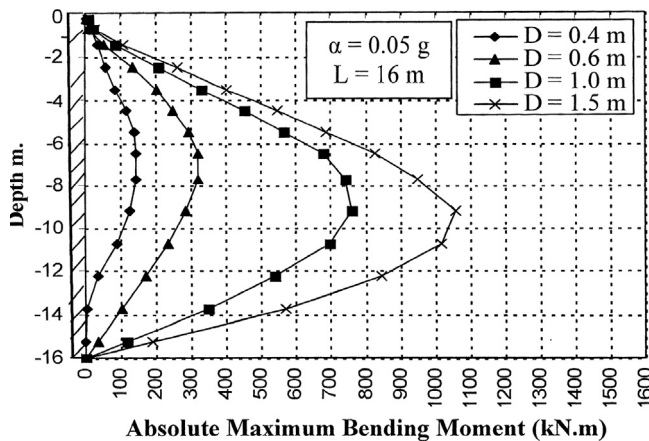

Figure 18 Bending moment profile along pile shaft (16.0 m length), under dynamic excitation of GEQ (II) and maximum base acceleration ($\alpha = 0.05$ g).
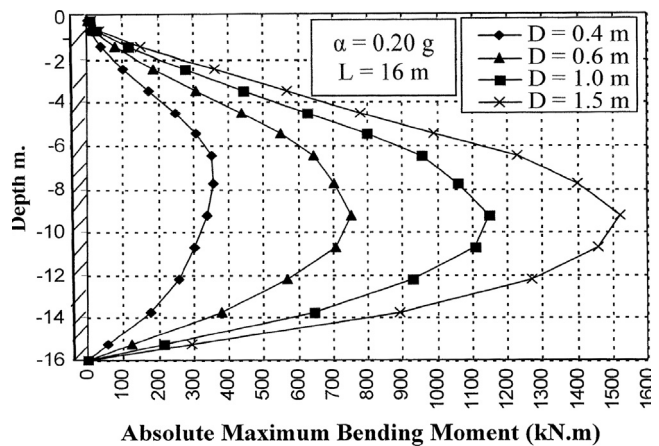

Figure 19 Bending moment profile along pile shaft (16.0 m length), under dynamic excitation of GEQ (II) and maximum base acceleration ($\alpha = 0.20$ g).

exerting moment curve and the flexural moment capacity determines the minimum needed pile diameter. Simply, if the ratio As/Ac equals 1.0 and considering ($\alpha = 0.20$ g), then the minimum needed pile diameter is 1.30 m. Upon examining these curves, the following can be established:

1. Selected pile diameter can be reduced using extra pile reinforcement, but it may increase the exerted lateral deformation. As mentioned before, this effect may be significant for small diameter and medium size piles (refer to Fig. 12).
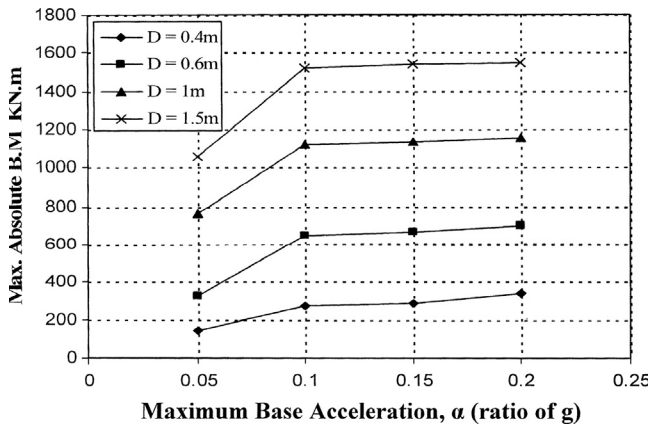
Figure 20 Relation between the maximum base acceleration and the absolute maximum bending moment, considering different pile diameters.
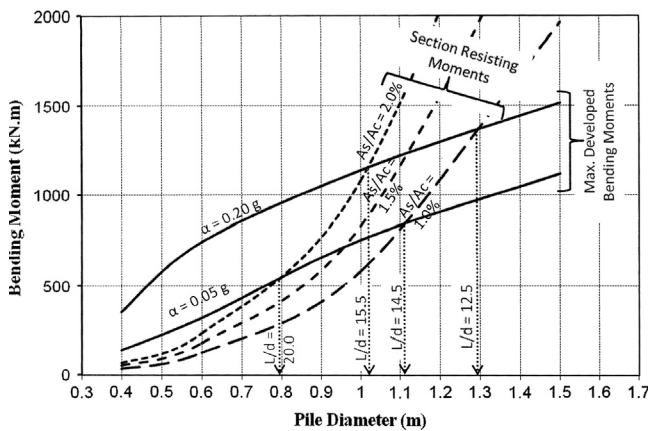

Figure 21 Relation between pile diameter and both developed bending moment and pile section resisting moment.

2. Considering recent study boundaries and studied parameter ranges, it is found that the needed pile diameters range between 0.80 and 1.30 m. This means that the ratio between pile length and diameter (L/D) ranges between 20.0 and 12.5, respectively.

3. Referring to Wahidy (2009) studies, it was established that if ($L/D < 30$), the stress acting on a pile is less than the Euler's stress, so buckling failure will not take place. Considering the above mentioned result in point (2), it is concluded that designing the reinforced concrete pile section to safely resist the developed bending moments may cover the risk of both buckling and plastic hinge mechanism.

7. Conclusions

In this study, an advanced numerical model has been used to simulate the sophisticated problem of the mutual seismic interaction between liquefiable loose sand formation and piles. The prepared numerical models are based on the finite element method using program DIANA 9.3 (2008). The proposed model is able to represent the soil–structure interaction system under seismic excitation and submerged conditions. Through

3D analysis, the pile is modeled as a beam element and the surrounding soil layers are modeled as solid elements. The model is supported by special 3 + 3 node Line–Solid Connection element, which is utilized to model the interface between the pile and the surrounding soil in three-dimensional configuration.

Extensive studies have been carried out to investigate the seismic interaction of the piles considering soil submergence conditions, pile diameter, length, earthquake magnitude and duration. The characteristics of the soil dealt with are cohesionless, having relative densities varying from loose to medium and up to very dense sand. Extensive studies have been carried out to investigate the seismic interaction of the piles considering pile diameter, earthquake magnitude and duration. Three generated artificial earthquakes records have been used as the control motion at the bed-rock surface. A practical wide range of maximum base acceleration is selected (α = 0.05, 0.10, 0.15 and 0.20 g), considering earthquake durations of 10, 20 and 40 seconds.

Both pile lateral deformation and developed bending moment along with pile shaft are studied. Recommendations and conclusions are presented to designer to avoid both buckling and plastic hinge failures. Study results yielded the following conclusions:

7.1. Lateral displacement of piles

1. In general, the lateral displacement of the pile due to seismic excitation is relatively high due to the low lateral resistance of the upper liquefiable loose sand formation. This observation is mentioned in all studied cases for both dry and fully saturated soil. The maximum lateral displacement of pile top of totally submerged case is usually greater than the full dry case. This observation can be clarified as the liquefaction of the loose sand causes a reduction in its shear resistance and consequently its lateral resistance (earth support).

2. Considering the deformation shape (lateral displacement) of piles, it is clear that the deformation of small diameter piles is highly affected by the developed flexural moment (behavior of horizontally loaded cantilever flexible pile). On the other hand, large pile results show the rigid body rotation pattern.

3. Pile diameter has a significant effect on reducing the lateral displacement, especially for relatively small and medium size pile diameters (up to 1.0 m diameter). For pile diameters greater than 1.0 m, the effect of pile diameter is limited. Accordingly, 1.0 m pile diameter may be considered as optimum size for such case study.

4. Lateral displacement is directly proportional to the maximum base acceleration (i.e., the earthquake associated energy), in a nonlinear behavior for both flexible and rigid piles.

5. Extensive studies have been carried out considering three different generated earthquake GEQ (I), GEQ (II) and GEQ (III) where the time periods are 10, 20 and 40 s, respectively. The following can be established:

   (i) There is a considerable difference between the results of using short time period, GEQ (I) and the other relatively long earthquake records, GEQ (II and III). It is concluded that ten (10) seconds may not be sufficient to reach the peak values of the pore water pressure ratio

r_u, especially in case of low base excitation ($\alpha = 0.05$ g). Accordingly, the generated dynamic water pressure is not sufficient to fully liquefy the soil and hence the soil does not completely lose its shear strength. As a result, the lateral displacement for such a case of short time duration recorded relatively low values of lateral deformations.

(ii) Considering the loose sand formation, it is clear that the dynamic energy of high base acceleration ($\alpha = 0.2$ g) could rapidly develop the dynamic water pressure and reach the full liquefaction situation after nearly 3 s. On the other hand, low base excitation could reach the same situation after relatively longer time (about 13 seconds).

(iii) For the lower medium dense sand formation, the condition of full liquefaction is not observed, where the values of ($r_u < 1.0$).

7.2. Developed bending moments along pile shaft

1. In general, the pattern of the exerted bending moment is similar to the bending moment diagram of cantilever wall. Its maximum value is located within the depth of the medium sand layer, where the soil passive resistance could be generated.

2. The exerted bending moment is highly related and directly proportional with pile diameter. This observation can be clarified as increasing pile diameter has two effects on the exerted bending moments. The first one concerns pile flexural rigidity and hence its capability to resist lateral deformation of the liquefied upper loose sand formation. The second effect is related to the increase of the contact area between the pile and soil and hence increasing the total mutual soil passive resistance, along with pile fixation length (at deep soil layers).

3. The maximum base acceleration has a considerable effect at zone of relatively low base acceleration (up to $\alpha = 0.10$ g). As mentioned before, these relatively low base accelerations have not sufficient dynamic energy to exert full liquefaction ($r_u < 1.0$). For higher values ($\alpha > 0.10$ g), full liquefaction ($r_u = 1.0$) could take place and hence no lateral resistance from the upper liquefied loose sand layer. On this condition, the effect of the earthquake magnitude is very limited, especially for large piles.

7.3. Expected failure mechanism

The maximum absolute bending moment along with pile shaft is compared with the flexural moment capacity of the pile section. Curves are plotted considering practical range of reinforcement ratio ($As/Ac = 1.0\%$, 1.5% and 2.0%). Examining these curves, the following can be established:

1. Selected pile diameters can be reduced using extra pile reinforcement, but it may increase the exerted lateral deformation.

2. Considering recent study boundaries and parameter ranges, it is found that the needed pile diameters range between 0.80 and 1.30 m. This means that the ratio between pile length and diameter (L/D) ranges between 20.0 and 12.5, respectively. Referring to Wahidy (2009) studies, it is established that for ($L/D < 30$), the stress acting on pile is less than the Euler's stress, so buckling failure will not take place. Considering study results, it is concluded that designing the reinforced concrete pile section to resist safely the exerted bending moments may cover the risk of both buckling and plastic hinge mechanism.

References

[1] Meyersohn WD. Pile response to liquefaction–induced lateral spread. Ph.D. Dissertation, Cornel University, Ithaca, NY; 1994.

[2] Amiri S. The earthquake response of bridge pile foundations to liquefaction induced lateral spread displacement demands, Ph.D. Dissertation, Faculty of the Graduate School, University of Southern California, USA; 2008.

[3] Popescu R, Prevost J. Comparison between VELACS numerical 'class A' predictions and centrifuge experimental soil test results. J Soil Dynam Earthquake Eng 1995;14(2):79–92.

[4] Wilson D, Boulanger R, Kutter B. Observed seismic lateral resistance of liquefying sand. J Geotech Geoenviron Eng 2000;126(10):898–906. ASCE.

[5] Bhattacharya S. Pile instability during earthquake liquefaction, Ph.D. Dissertation, University of Cambridge, UK; 2003.

[6] Ashour M, Norris G. Lateral loaded pile response in liquefiable soil. J Geotech Geoenviron Eng 2003;129(6):404–14. ASCE.

[7] Abdoun T, Dobry R, O' Rourke T, Goh SH. Pile response to lateral spreads: centrifuge modeling. J Geotech Geoenviron Eng 2003;129(10):869–78. ASCE.

[8] Ilyas T, Leung C, Chow Y, Budi S. Centrifuge model study of laterally loaded pile groups in clay. J Geotech Geoenviron Eng 2004;130(3):274–83. ASCE.

[9] Rollins MK, Gerber MT, Lane DJ, Ashford AS. Lateral resistance of a full – scale pile group in liquefied sand. J Geotech Geoenviron Eng 2005;131(1):115–25. ASCE.

[10] Weaver T, Ashford S, Rollins K. Response of 0.6 m cast-in-steel-shell pile in liquefied soil under lateral loading. J Geotech Geoenviron Eng 2005;131(1):94–102.

[11] Wahidy M. Stability of piles penetrated into liquefiable soil under seismic excitation, Ph.D. Dissertation, Faculty of Engineering, Ain Shams University, Cairo, Egypt; 2009.

[12] DIANA Finite Element Analysis, User's Manual, Release 9.3. TNO DIANA BV, Schoemakerstraat 97, 2628 VK Delft, Netherlands; 2008.

[13] Madabhushi J, Knappett J, Haigh S. Design of pile foundations in liquefiable soils. London, UK: Imperial College Press; 2010.

[14] Li P, Ma D, Zeng D, Lu X. Numerical simulation of pile–soil interaction considering sand liquefaction under earthquake. Appl Mech Mater 2012;226–228:1019–22.

[15] Seed HB, Lysmer J, Hwang R. Soil–Structure interaction analyses for seismic response. J Geotech Eng 1975;101(GT5):439–57. ASCE.

[16] Lysmer J, Udake T, Tsai C-F, Seed HB. Computer program for approximate 3-D analysis of soil–structure interaction problem. Report No. EERC 75–30, College of Engineering, University of California, Berkeley, California; 1975.

[17] Macky T, Mokhtar A, Fayed M, Abdel-Motaal M. Controlling the dynamic response of structures using foundation ties. In: 8th

Int colloquium on struct and geotech eng, Ain Shams University, Cairo, Egypt; 1998.

[18] Abdel-Motaal M. Soil effect on the dynamic behavior of framed structures. Ph.D. Dissertation, Faculty of Engineering, Ain Shams University, Cairo, Egypt; 1999.

[19] Abdel-Motaal M. Seismic response of underground station during construction stages. In: 9th Int colloquium on struct and geotech eng, GE-25, Ain Shams University, Cairo, Egypt; 2001.

[20] Mokhtar A, Abdel-Motaal M, Wahidy M. Stability of piles penetrated into liquefiable soil under seismic excitation. Ain Shams J Civil Eng Egypt 2010;1:173–83.

[21] Ohtsuki K, Yokoyama K, Sato M, Fukutake K. Shaking table test and 2D nonlinear analysis for sand-structure system. In: 10th World conference, earthquake engineering, Balkema, Rotterdam; 1992. p. 1865–71.

[22] Uzuoka R, Cubrinovski M, Sugita H, Sato M, Tokimatsu K, Sento N, Kazama M, Zhang F, Yashima A, Oka F. Prediction of pile response to lateral spreading by 3-D soil-water coupled dynamic analysis: shaking in the direction perpendicular to ground flow. J Soil Dynam Earthquake Eng 2008;28(6):436–62.

[23] Tolon M. A comparative study on computer aided liquefaction analysis methods. Int J Housing Sci 2013;37(2):121–35, USA.

[24] The Egyptian Code of Soil Mechanics and Foundation Design, Code (202/2001), HBRC, Giza, Egypt; 2001.

Mohamed Ahmed Abdel-Motaal works as Associate Professor of Geotechnical Engineering at the Departement of Structural Engineeering Ain Shams University, Cairo Egypt. Since April 2012, he was appointed as director of Soil Mechanics and Foundation Engineering Consulting Unit (SMFU) at Ain Shams University. He is a member of the experts' board for updating the Egyptian Code of Soil Mechanics and Foundation Design (Part 6). His research interest is Soil Dynamics, Dynamic-Soil-Structure Interaction, Geotechnical Earthquake Engineering and Soil Stabilization.

Mohamed Mustafa Wahidy is General Manager for Building Execution at the Egyptian Company for Telecommunication. He got his Ph.D. in Geotechnical Engineering from Ain Shams University. His research interests include soil dynamics, liquefaction and dynamic Soil-Structure interaction.

Abdel-Salam A. Mokhtar is Professor of Structural Engineering at Ain Shams University. His research interests include nonlinear analysis, dynamics of structures and soil-structure interaction.